A stress-induced response complex (SIRC) shuttles miRNAs, siRNAs, and oligonucleotides to the nucleus

Daniela Castanotto[a,1], Xiaowei Zhang[a], Jessica Alluin[b], Xizhe Zhang[c], Jacqueline Rüger[a], Brian Armstrong[d], John Rossi[b], Arthur Riggs[c], and C. A. Stein[a,b,1]

[a]Department of Medical Oncology, City of Hope, Duarte, CA 91010; [b]Department of Molecular and Cellular Biology, City of Hope, Duarte, CA 91010; [c]Department of Diabetes & Metabolic Diseases, City of Hope, Duarte, CA 91010; and [d]Department of Neuroscience, City of Hope, Duarte, CA 91010

Edited by Marvin H. Caruthers, University of Colorado at Boulder, Boulder, CO, and approved May 7, 2018 (received for review December 11, 2017)

Although some information is available for specific subsets of miRNAs and several factors have been shown to bind oligonucleotides (ONs), no general transport mechanism for these molecules has been identified to date. In this work, we demonstrate that the nuclear transport of ONs, siRNAs, and miRNAs responds to cellular stress. Furthermore, we have identified a stress-induced response complex (SIRC), which includes Ago-1 and Ago-2 in addition to the transcription and splicing regulators YB1, CTCF, FUS, Smad1, Smad3, and Smad4. The SIRC transports endogenous miRNAs, siRNAs, and ONs to the nucleus. We show that cellular stress can significantly increase ON- or siRNA-directed splicing switch events and endogenous miRNA targeting of nuclear RNAs.

miRNA | SSO | stress granules | FUS | YB1

MicroRNAs (miRNAs), siRNAs, and chemically modified oligonucleotides (ONs) have been employed for many years for research and, increasingly, for therapeutic purposes (1). miRNAs, which may control the expression of more than half of all human genes, are active predominantly in the cytoplasm, but they also form complexes in the cell nuclei with components of the RNAi machinery (2). Various regulatory nuclear functions have been attributed to miRNAs and other noncoding RNAs (ncRNAs), including the much-debated question of transcriptional gene silencing (3). Similarly, ONs delivered by gymnosis (4) are active in the cytoplasm (5), and can also be transported to and are effective in the nucleus (5, 6). Although various candidate proteins have been reported to bind ONs (5, 7, 8), the mechanism that determines whether a miRNA or an ON exerts its function in the cytoplasm or shuttles to the nucleus and acts at an earlier step in the gene regulation pathway is unknown. It is also unclear if the nuclear/cytoplasmic shuttling of these small molecules is a continuous endogenous process or if it is the result of a specific signal.

We previously demonstrated that ONs can utilize elements of endogenous miRNA pathways to optimize function. This is due to their ability to bind to the RNA-induced silencing complex (RISC) components such as Argonaute-2 (Ago-2) (5). Although Ago-2 can affect ON function, the degradation products of ON-targeted RNAs are not generated by Ago-2–directed cleavage. We concluded that Ago-2 is employed by the ONs as a method of transport and localization to RNA targets. This is supported by our observations that when ONs were delivered via gymnosis (4), their mode of uptake and cellular localization seemed to be identical to that of siRNAs (5). Therefore, ONs could be employed to identify protein complexes and mechanisms used by exogenous siRNAs and, most importantly, endogenous miRNAs.

In this work, ONs have been used to identify a complex consisting of transport proteins, splicing regulators, and transcription factors bound to the ONs and, in addition, to miRNAs. The formation and nuclear translocation of this complex increase subsequent to cellular stress. This cytoplasmic/nuclear shuttling brings the associated miRNA (and ONs) to the nucleus, where they are functional and can potentially alter gene expression and participate in cell stress response mechanisms. We also show that inducing a cell stress response by adding small, clinically relevant concentrations of arsenite [arsenic trioxide (As III)] results in greatly increased ON, siRNA, or miRNA targeting and suppression of nuclear RNAs, demonstrating the validity of our findings. The fine-tuning of this process may be of extreme importance for the manipulation of miRNAs, siRNAs, and ONs in a therapeutic setting.

Results

ONs Bind Shuttling Proteins That Are Involved in the Cell Stress Response. We previously demonstrated that ONs delivered by gymnosis (ON delivery to cells that produces function in the absence of any carriers or conjugations) are bound by Ago-1–Ago-4 (5) and may utilize multiple endogenous mechanisms employed by cellular miRNAs. Ago-2 binding augments ON function, which we proposed was due to Ago-2 facilitation of ON transport (5). We speculated Ago-2 could be part of a transport complex that differed from RISC.

To test the hypothesis that ONs were bound to an Ago-2 transport complex and to identify additional proteins belonging to this complex, we performed immunoprecipitations (IPs) of Ago-1 or Ago-2 using cell lysates harvested from HEK293 cells that were (*i*) untreated, (*ii*) treated with a control ON delivered by gymnosis, or (*iii*) transfected with a control siRNA. All of the ONs used in our studies are phosphorothioate (PS), locked nucleic acid (LNA) gapmer (3′ and 5′ end sugar modifications),

Significance

The deregulation of miRNA function is critical in the pathogenesis of cancer and other diseases. miRNAs and other noncoding RNAs (ncRNAs) tightly regulate gene expression, often in the cell nucleus. Heretofore, there has been no understanding that there exists a general shuttling mechanism that brings miRNAs, in addition to therapeutic oligonucleotides and siRNAs, from the cytoplasm into the nucleus. We have identified this shuttling mechanism, which occurs in response to cell stress. Nuclear imported miRNAs are functional, can potentially alter gene expression, and participate in cell stress response mechanisms. This shuttling mechanism can be augmented to target specific RNAs, including miRNA sponges, and long ncRNAs like Malat-1, which have been implicated in promoting tumor metastasis.

Author contributions: D.C. and C.A.S. designed research; D.C., Xiaowei Zhang, J.A., Xizhe Zhang, and J. Rüger performed research; B.A. and J. Rossi contributed new reagents/analytic tools; D.C., A.R., and C.A.S. analyzed data; B.A. assisted with microscopy imaging; and D.C. and C.A.S. wrote the paper.

The authors declare no conflict of interest.

This article is a PNAS Direct Submission.

This open access article is distributed under Creative Commons Attribution-NonCommercial-NoDerivatives License 4.0 (CC BY-NC-ND).

[1]To whom correspondence may be addressed. Email: dcastanotto@coh.org or cstein@coh.org.

This article contains supporting information online at www.pnas.org/lookup/suppl/doi:10.1073/pnas.1721346115/-/DCSupplemental.

Published online June 4, 2018.

or mixmer (alternating sugar modifications) ONs (9, 10) (all PS-LNA-ONs are indicated as ONs), which increase stability and cellular uptake by gymnosis. We performed a mass spectrometric analysis of the precipitates and analyzed only those proteins that were common in both lysates of cells treated with the control siRNA and lysates treated with the ON but were absent in all other samples and controls. Under our experimental conditions, apart from ribosomal proteins, tubulin, and immunoprecipitated Argonautes, we found nucleolin, SRSF1, and six splicing factors (YB1, DbpA, PABP1, HSP-70, KIF11, and elongation factor 1α) (Dataset S1). Nucleolin is a shuttling protein (11) that has been previously reported to bind ONs (7). SRSF1 and SRSF7 are members of the SR protein family, which has been shown to act on nuclear export factor 1 (NXF1) (12). The heat shock protein HSP-70 is a chaperone, stress-response protein that, among other functions, increases the stability of nucleolin during oxidative stress (13), and it is known to associate with YB1 during stress (14). YB1 is involved in a myriad of cellular functions; it is also a chaperone and a key player in the cellular stress response, which leads to its translocation into the nucleus (15). YB1 is also involved in stress granule (SG) formation, where it localizes (14). DbpA (YBX3) is also a Y-box binding protein (16, 17), while PABP1 binds to the mRNA poly(A) tail and is important in mRNA translation and nonsense-mediated decay. PABP1 also concentrates in SGs (18). KIF11 is a kinesin-related protein that plays a role in cell division and enhances the efficiency of mRNA translation (19). Elongation factor 1α also plays a role in translation and, in addition, a central role in the nuclear export of proteins (20). Therefore, nearly all of the proteins identified are involved in transport and in the cellular stress response.

In this context, we found nucleolin and YB1 to be of special significance. Nucleolin is known to bind ONs (7) but has not been previously shown to bind siRNAs. However, it has been reported to interact with the microprocessor complex and to affect the processing of specific miRNAs (21).

We proceeded to confirm the binding of these two proteins to the Argonautes by immunoprecipitation and immunoblotting with specific antibodies (Fig. 1 *A* and *B*).

Next, as most of the factors identified in our mass spectrometric assay, including Ago-1 and Ago-2, are known to shuttle from the cytoplasm to the nucleus (3), we employed tetracycline (Tet)-inducible stable cell lines expressing anti–Ago-shRNAs (22) to study the effects of Argonaute (Ago-1, Ago-2, or Ago-3) depletion on ON cellular localization (Fig. 1*C* and *SI Appendix*, Fig. S1 *A* and *B*). The nuclear-to-cytoplasmic RNA ratio can be compared, after loading the samples, either by volume (samples suspended in equal amounts of loading buffer) or by weight (equivalent number of micrograms of sample loaded, which is shown in this experiment). However, neither of these methods represents the entire amount of RNA in each of these cellular compartments. Furthermore, it is inevitable that some of perinuclear cytoplasmic components will be precipitated with the nuclear fraction. The nuclear and cytoplasmic fractionations shown in this work were analyzed based on changes in the relative ratio between the two fractions, rather than on the absolute amount of signal detected in each fraction. The analysis of three independent experiments is shown in *SI Appendix*, Fig. S1*B*.

Down-regulation of Ago-2, but not Ago-1 or Ago-3, resulted in ON localization that favors the cytoplasmic compartment [Fig. 1*C*, compare Ago-2 (Dox^-) with Ago-2 knockdown (Ago-2 kd) (Dox^+) versus Ago-1 or Ago-3 (Dox^-) with Ago-1 kd or Ago-3 kd (Dox^+), respectively]. Down-regulation of the Argonautes following Tet induction in these cell lines has been previously validated by us and others (22).

Delivery of ONs by Gymnosis Results in Increased Ago-2/YB1 Complex Formation. Some reports have indicated an active role for nucleolin in the binding of ONs (23), but others have not been able to find a functional role for it in ON activity (8). It is possible that nucleolin either has a redundant function or that its contribution to ON function is measurable only in certain cell systems and under specific experimental conditions (24). Subsequent to downregulating nucleolin expression by an siRNA approach, and consistent with these observations, we detected only a marginal effect (up to 30%) on ON function, and then only if ONs were delivered by gymnosis rather than by lipofection. Therefore, we focused on the role of YB1, which we also found in the Ago/ON immunoprecipitated complexes. We performed additional IP experiments that complemented the original Ago IPs by using HeLa cell lysates and a YB1 antibody to confirm (*i*) the interaction of YB1 with Ago-1 and/or Ago-2 (Fig. 2*A*), and (*ii*) the increase of this interaction on the presence of the ON (Fig. 2*B*). Both Ago-1 and Ago-2 proteins immunoprecipitated with the anti-YB1–specific antibody (Fig. 2 *A* and *B*). Strikingly, the amount of Ago-2, but not Ago-1, in the YB1 immunoprecipitates increased when cells were treated with ONs delivered by gymnosis (compare Fig. 2 *A*, *Bottom*, Ago-1, Ago-2, and YB1 lanes with *B*, *Bottom*, Ago-1, Ago-2, and YB1 lanes).

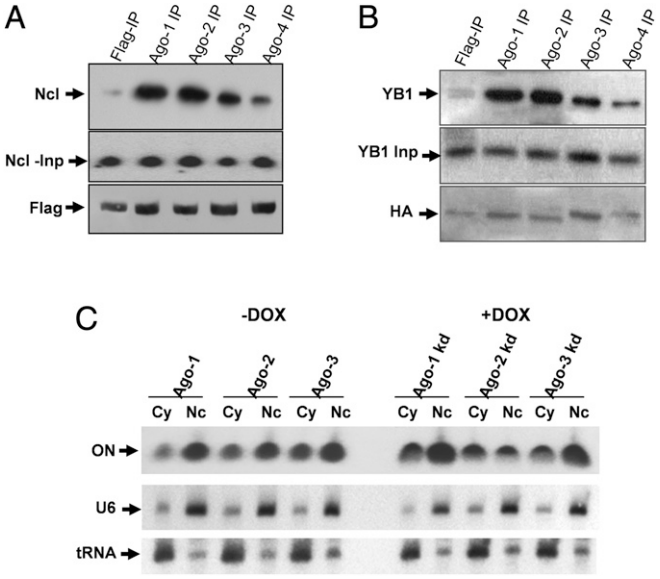

Fig. 1. Ago-2 appears to shuttle ONs into the nucleus and forms a complex with the nucleolin and YB1 proteins. (*A* and *B*) IP reactions were performed with an anti-Flag antibody employing lysates of cells stably expressing the Flag-HA–tagged Ago-1–Ago-4 (as indicated) or the Flag-HA vector control. Nucleolin and YB1 proteins are detected in the Ago-Flag cells but not in the control cells. The starting input for each IP is shown [nucleolin (Ncl)-Inp and YB1-Inp]. Immunoblotting of Flag and HA was used to determine the efficiency of the IP for each sample. (*C*) ON was delivered by gymnosis to Tet-inducible stable cell lines expressing anti–Ago-shRNAs specific for the Ago-1, Ago-2, or Ago-3 sequence. Doxycyclin (+DOX) was added to induce expression of the shRNA and silencing of Ago-1–Ago-3 expression. The cytoplasmic (Cy) and nuclear (Nc) fractions are shown. The U6 snRNA (U6), which is localized to the nucleus, and cytoplasmic tRNA (tRNA) were used as controls. The verification of Argonaute silencing under these experimental conditions is shown in *SI Appendix*, Fig. S1*A*.

Ago-2 and YB1 Directly Interact as a Consequence of Cellular Stress and Colocalize in the Same Cellular Compartments. To determine whether a direct interaction between YB1 and Ago-2 occurred, we conducted proximity ligation assays (PLAs) (25, 26) using YB1 and Ago-1 or Ago-2 with PLA antibodies (which are primer-conjugated; Fig. 2 *D*–*F*). The simultaneous double recognition by the mixed probes required to obtain a fluorescence signal is highly selective and specific for protein recognition and protein–protein interaction (25, 26). The fluorescence signal detected in the sample

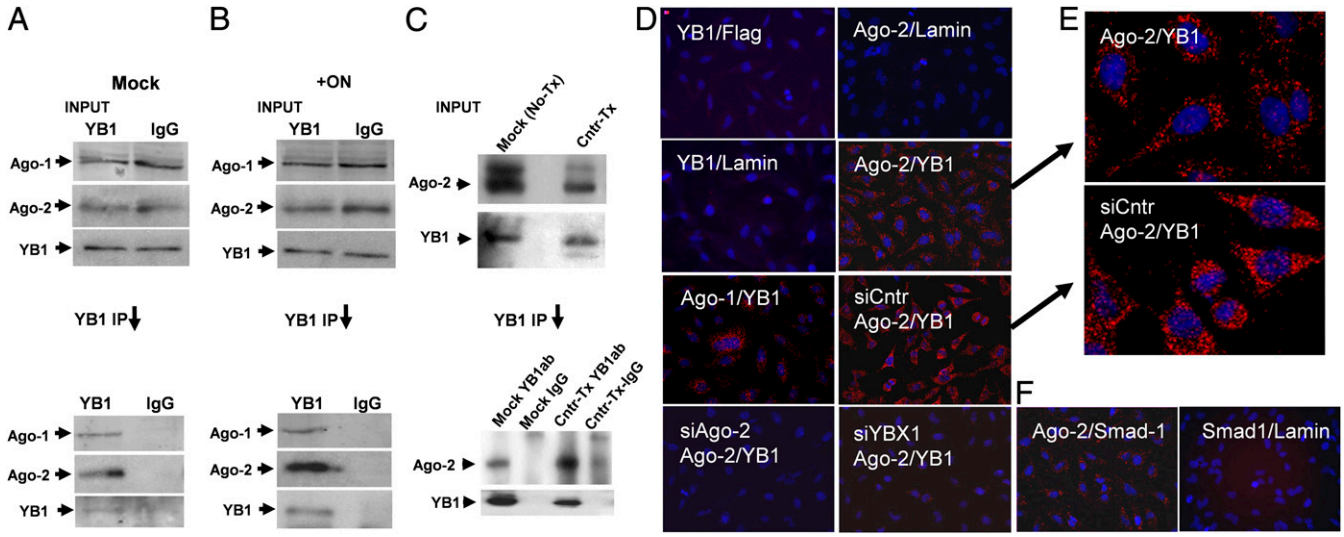

Fig. 2. YB1 forms a complex with Ago-2, which is increased by cellular stress. (*A–C*, *Bottom*) IP of YB1 from HeLa lysates reveals the presence of Ago-1 and Ago-2 in the complex as indicated by the arrows. Lysates were collected 48 h subsequent to initiation of gymnosis. The association of Ago-2 increases when stress is induced by adding an ON (+ON; *B*) or by lipofection [transfection (Tx); *C*]. (*A–C*, *Top*) Ago-1, Ago-2, and YB1 inputs are shown. Mock represents untreated cells (no ON). IgG was used as the IP control. (*D–F*) Antibody primers specific for YB1, Flag, Ago-1, Ago-2, Lamin, and Smad1 (the specific pairings are shown) were used in a PLA reaction. (*E*, *Bottom*) Adding a control nontargeting siRNA (siCntr) augments the red fluorescence signal, indicating increased colocalization of Ago-2 and YB1. Blue shows DAPI-stained nuclei. (Magnification: 400×.) Enlargements of the panels showing positive signals are provided in *SI Appendix*, Fig. S2.

treated with the Ago-2– and YB1-specific probes (Fig. 2*D*, Ago-2/YB1), but not in the controls [Fig. 2*D*; anti-YB1 and anti-Flag antibodies (YB1/Flag), anti–Ago-2 and anti-Lamin antibodies (Ago-2/Lamin), and anti-YB1 and anti-Lamin antibodies (YB1/Lamin)], supported a direct interaction between Ago-2 and YB1 and demonstrated intracellular colocalization in the perinuclear region and in the cell nucleus (Fig. 2 *D* and *E*). The signal, when the anti–Ago-1– and anti-YB1–specific mixed probes were employed, was present but reduced relative to Ago-2/YB1 (Fig. 2*D*, compare Ago-2/YB1 with Ago-1/YB1). This supports a close, although not necessarily a direct, interaction. To further validate the specificity of the PLAs and the reliability of these results, Ago-2 and/or YBX-1 (the gene producing YB1) expression was silenced with specific siRNAs (*SI Appendix*, Fig. S3 *A* and *B*, siAgo-2 and siYBX-1). Down-regulation of these genes was verified by Western blot (*SI Appendix*, Fig. S3*A*) and qPCR analyses (*SI Appendix*, Fig. S3*B*) before performing the PLAs. Fluorescent signal was lost (Fig. 2*D*) when the expression of either protein (Ago-2 or YB1) was silenced [Fig. 2*D*, compare Ago-2/YB1 and siCntr (control) Ago-2/YB1 with siAgo-2 Ago-2/YB1 or siYBX1 Ago-2/YB1].

A more intense fluorescent signal was detected for the Ago-2/YB1 interaction in the siRNA control sample (siCntr Ago-2/YB1), which underwent transfection. Following this stress signal that was triggered by lipofection, we observed an increased interaction between these two proteins, consistent with the IP results (Fig. 2 *A* and *B*). This Ago-2/YB1 interaction also resulted in an increased nuclear accumulation of this complex in nuclear speckles, as seen in Fig. 2*E*, which shows a magnified view of the Ago-2/YB1 PLA results with or without transfection of the siRNA control.

To examine if the interaction between Ago-2 and YB1 was a general response to stress or specific only to the delivery of siRNA and ONs, we performed YB1 IPs after lipofecting an empty plasmid backbone into HEK293 cells (Fig. 2*C*). Lipofection alone was sufficient to increase the association of Ago-2 and YB1 [Fig. 2*C*, compare the ratios between the immuno-precipitated YB1 and the amount of bound Ago-2 in the Mock (Mock YB1ab) vs. control transfected cells (Cntr-Tx-YB1ab)].

YB1, Ago-2, and the miRNA machinery are involved in the cellular stress response (27, 28). Furthermore, YB1 has been shown to be important in the regulation of the Smad-signaling pathway (29). Smad transcription factors are a critical piece of one of the most multifaceted cytokine signaling pathways: the transforming growth factor-β pathway (30). Once activated by phosphorylation, these proteins translocate to the nucleus, where they regulate gene expression (30). Therefore, we hypothesized that they are also potential partners of the stress-induced YB1/Ago-2 complex. To determine if Ago-2 also interacts with the Smad complex, we performed a PLA with Smad-1– and Ago-2–specific mixed probes. The fluorescent signal detected (Fig. 2*F*) supports that a direct or indirect interaction is occurring.

We then examined protein kinase R (PKR) activation under our experimental conditions. PKR is at the center of the stress response pathway. The delivery of ONs by gymnosis triggers an increase in PKR expression as a function of time and ON concentration (*SI Appendix*, Fig. S4).

Cellular Stress Increases siRNA and ON Function in the Nucleus and Concomitantly Reduces Their Function in the Cytoplasm. To establish if this increased interaction between Ago-2 and YB1 translated to augmented ON function, we delivered a splice-switching ON (SSO-654) by gymnosis to the HeLa-EGFP-654 cell line (31), which was either untreated or previously lipofectamine-transfected with a stressor (in this case, a nontargeting siRNA). The SSO-654 was designed to induce skipping of an exon that disrupts the EGFP coding sequence expressed in these cells; therefore, the potency of this SSO is directly proportional to the signal of the EGFP that is produced (31), and thus is a measure of ON function in the nucleus. The stress induced by the siRNA transfection resulted in more effective splicing switch activity and higher EGFP expression at three different SSO-654 concentrations [*SI Appendix*, Fig. S5*A*; compare 0.5 μM, 1 μM, and 2 μM SSO-654 in non-transfected HeLa-EGFP-654 cells (Mock) and HeLa-EGFP-654 cells transfected with a nontargeting siRNA (40 nM siCntr) before ON delivery]. The improvement in SSO-654 activity was also observable at an early time point (24 h) following SSO-654 delivered by gymnosis, and with a lower concentration (10 nM) of the nontargeting transfected siRNA control (*SI Appendix*, Fig.

S5*B*, 10 nM siCntr) or with uncomplexed lipofectamine (*SI Appendix*, Fig. S5*B*, Lip only). The enhancement of ON function increased with time (*SI Appendix*, Fig. S5*B*, *Lower*, Gymnosis 48 hrs).

The increase in ON function could be recapitulated with As III, a standard cellular stressor. We chose As III, although it can cause oxidative damage (32), because at the appropriate concentrations, it also has therapeutic properties (33, 34). We found that SSO-654 potency improved, as determined by EGFP production in HeLa-EGFP-654 cells, when low concentrations (0.5–2 μM) of As III were combined with SSO-654 treatment (Fig. 3 *A* and *B*).

We confirmed the increased production of EGFP as a function of the As III concentration (1 and 2 μM) by microscopy and flow cytometry measurements (*SI Appendix*, Fig. S6 *A–C*). We also quantified EGFP protein expression by Western blot analyses at two SSO-654 concentrations (*SI Appendix*, Fig. S6*B*). Finally, to exclude the possibility that the enhanced SSO-654 function was due to changes in ON uptake or cell viability, we evaluated (*i*) the efficiency of ON delivery by gymnosis in two separate cell lines (*SI Appendix*, Fig. S7*A*, HeLa-EGFP-654 and *SI Appendix*, Fig. S7*B*, LNCaP) in untreated cells or cells treated with As III (1 μM) and (*ii*) the viability of HeLa-EGFP-654 cells treated with the SSO-654 alone or in combination with As III (*SI Appendix*, Fig. S7 *C* and *D*). No significant changes in ON uptake or cell viability were detected when cells were treated with ONs in combination with As III (*SI Appendix*, Fig. S7 *A–D*). These data corroborated that the increased ON potency is related to a general cellular stress response. Indeed, additional cell stressors, such as hydrogen peroxide (H_2O_2) or heat shock, also increased SSO-654 function (*SI Appendix*, Fig. S8), in addition to causing increased PKR expression (*SI Appendix*, Fig. S9). Cold shock, which does not significantly trigger cellular stress, was used as a control and did not activate PKR (*SI Appendix*, Fig. S9) or increase SSO-654 potency (*SI Appendix*, Fig. S8). Notably, treatment with ammonium ions (NH_4^+) did not elicit a PKR response (*SI Appendix*, Fig. S9) but still increased the potency of SSO-654 (*SI Appendix*, Fig. S8) and PS-LNA antisense ONs (35). We hypothesized that NH_4^+ potentiates ON activity via a different mechanism than As III. Because two separate pathways leading to ON activation seem to exist, combining both compounds (As III and NH_4^+) resulted in a synergistic increase in ON function (35).

Nuclear Translocation of YB1 Coincides with Increased RNAi and ON Potency. The increased potency of SSO-654 was a reflection of its increased concentration in the nuclear compartment and coincided with the nuclear translocation of YB1. We performed nuclear/cytoplasmic fractionations of the HeLa-EGFP-654 cells treated with ONs with or without As III. As III induces accumulation of YB1 in the nucleus [Fig. 4*A*, compare the YB1 ratio between the cytoplasmic and nuclear fractions in cells treated with ONs but not As III (−) and the same fractions from lysates of As III-treated cells (+)]. The nuclear translocation of YB1 after As III treatment corresponds to concomitant accumulation of ONs in the nucleus (Fig. 4*B*). It has been shown that YB1 can bind to and regulate the biogenesis of specific miRNAs (36), and that its interaction with Ago-2 increases during cellular stress (this work). We have also previously shown that ONs behave similar to siRNAs, and may hijack endogenous siRNA/miRNA cellular pathways (5). Therefore, we investigated whether the nuclear translocation and improvement in function observed using ONs in the stress condition could be recapitulated with siRNA and miRNA. We performed an IP using anti-YB1–specific antibodies,

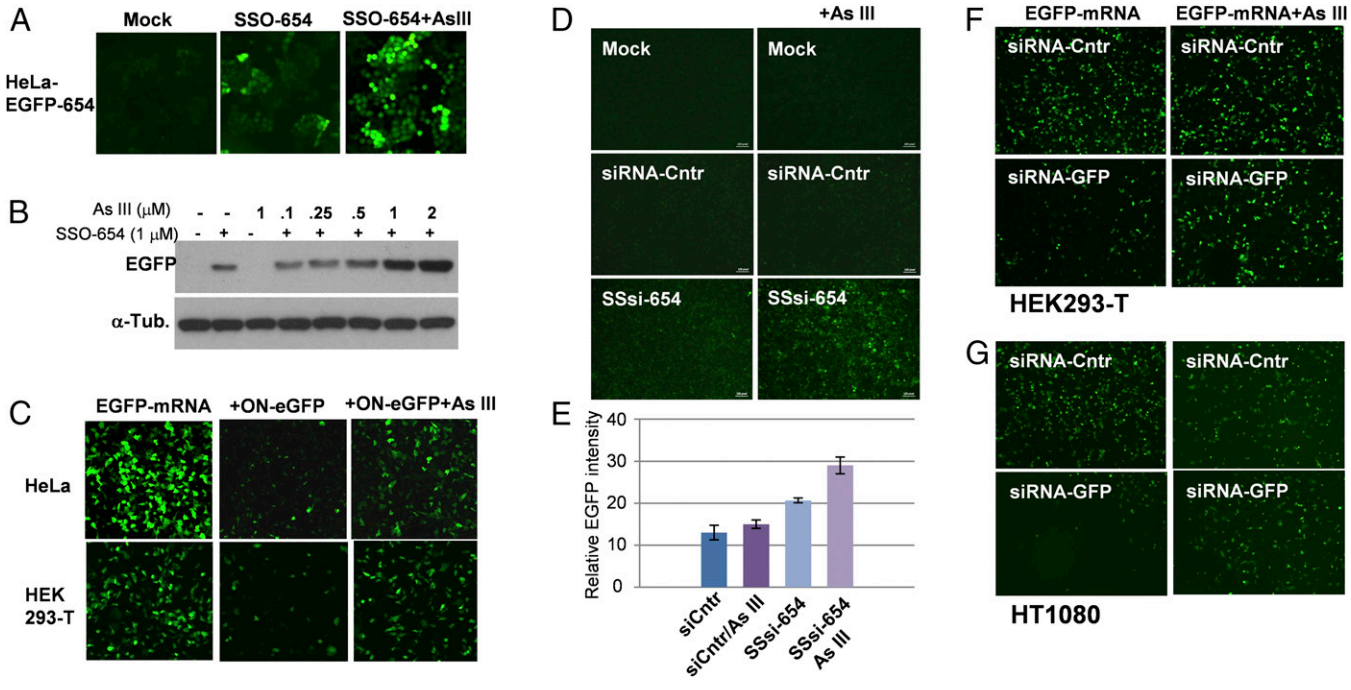

Fig. 3. Stress-induced As III treatment increases nuclear function and concomitantly decreases the cytoplasmic function of ONs and siRNAs. (*A*) SSO-654 was delivered by gymnosis to HeLa-EGFP-654 cells with or without As III before fluorescent microscopy. (*B*) Western blot analysis of HeLa-EGFP-654 treated with 1 μM SSO-654 and increasing concentrations of As III, as indicated, for 2 d. α-Tub., α-Tubulin. (*C*) Anti-EGFP ON (+ON-EGFP) was delivered by gymnosis to HeLa (*Top*) and HEK293-T (*Bottom*) cells before the transfection of EGFP mRNA. *Right* panels show As III (+ON-EGFP + As III)-treated cells. (*D*) SSsi-654 was transfected to HeLa-EGFP-654 cells with or without As III (+As III) before fluorescent microscopy. A control nontargeting siRNA (siRNA-Cntr) is shown. (*E*) Graph represents the combined analysis of three different experiments, including three technical replicates. The fluorescent signal was quantified over the entire surface of wells containing equivalent number of cells with Image Pro Premier 9.2. (*F* and *G*) HEK293-T (*Top*) and HT1080 (*Bottom*) (EGFP-mRNA)–treated cells (EGFP-mRNA) were transfected with an anti-EGFP siRNA (siRNA-EGFP) or a nontargeting control (siRNA-Cntr). *Right* shows As III (EGFP-mRNA + As III)-treated cells. (Magnification: 180×.)

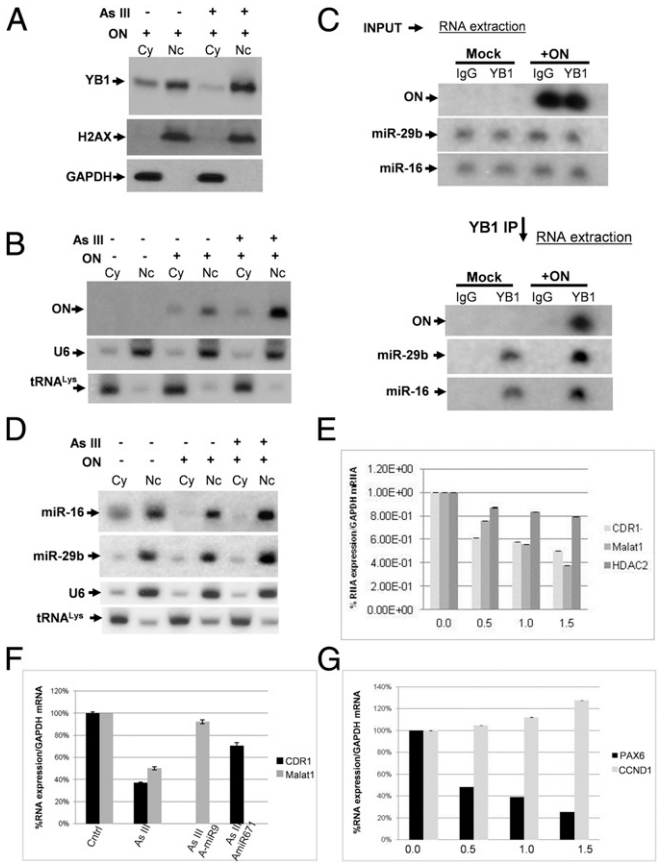

Fig. 4. Cellular stress promotes the nuclear translocation of a YB1 complex containing miRNAs, siRNAs, and ONs. Nuclear (Nc) and cytoplasmic (Cy) fractions of HeLa cells with (+) or without (–) As III and ON treatment, followed by (*A*) Western blot analysis and (*B* and *D*) Northern blot analysis for the detection of YB1 (*A*), ON (*B*), or miR16 and miR29b (*D*). Antibodies specific for H2AX and GAPDH were used to assess the purity of the protein fractions, and γ-^{32}P–labeled probes base-pairing to the U6 snRNA and tRNA^{lys} were used for the RNA/ON fractions. (*C*) Northern analysis of RNA and ON extracted from YB1 immunoprecipitated samples (YB1 IP) that were harvested from lysates of untreated (Mock) or treated (+ON) HeLa cells. The starting input for the IPs is shown. The γ-^{32}P–labeled probes were used to detect ON, miR29b, and miR16 as indicated. (*E*) RT-PCR detection of the reduction of miR671- and miR9-regulated nuclear RNA target (CDR1 and Malat-1, respectively) levels in HEK293-T cells treated with different concentrations (0.5 μM, 1 μM, and 1.5 μM) of As III. Amplification of a miRNA-regulated cytoplasmic target (HDAC) was used as a control and did not significantly change at 1 μM and 1.5 μM As III concentrations (Student's *t* test, compared with untreated control and based on the mean value ± SD; $n = 3$; $P = 0.0002$ and $P = 0.012$, respectively). (*F*) RT-PCR detection of CDR1 and Malat-1 expression levels in HEK293-T cells treated with As III (1.5 μM) and either an miR9- or miR671-specific miRNA antagomir. Cntrl, Control. (*G*) RT-PCR detection of the expression levels of the miR7 cellular targets PAX6 and CCND1 in HEK293-T cells treated with increasing concentrations (0.5 μM, 1 μM, and 1.5 μM) of As III. Graphs represent three technical replicates. Three biological replicates were performed in triplicate for each treatment. Consistent results were obtained.

extracted the nucleic acids from the lysate precipitates of untreated cells (Mock) or cells treated with 1.5 μM ON (+ON), and performed a gel analysis. An increased association of three separate miRNAs (two, miR-29b and miR-16, are shown; miR-21 followed the same pattern but is not included in the figure) with the YB1-precipitated complex was observed when cells were previously treated with the ON [Fig. 4*C*, compare miR-29b and miR-16 in the Mock (YB1 lane) vs. in the +ON (YB1 lane)]. We then performed nuclear/cytoplasmic fractionations of untreated cells or cells treated with the ON, or with a combination of the ON and As III. Shuttling of the miRNAs to the nucleus increased proportionally to the extent of the stress signal [Fig. 4*D* and *SI Appendix*, Fig. S10, compare the miRNA ratio of the cytoplasmic and nuclear fractions of untreated cells (lanes 1 and 2) with those of cells treated with the ON (lanes 3 and 4) and cells treated with a combination of the ON and As III (lanes 5 and 6)].

To verify that the augmented nuclear shuttling of miRNAs translated into their increased activity in the nucleus, we designed a splice-switching siRNA (SSsi-654) with the same sequence as SSO-654. This is a canonical siRNA, and thus functions primarily in the cytoplasm; however, we were still able to detect splice-switching activity in the nucleus (Fig. 3 *D*, first column, compare siRNA-Cntr with SSsi-654 and *E*). This nuclear function can be increased by As III treatment (Fig. 3 *D*, +As III and *E*), indicating that shuttled mature siRNA/miRNA is active in the nucleus.

The augmentation of nuclear targeting by the nuclear-translocated siRNAs or ONs is expected to occur with a concomitant decrease of their cytoplasmic function. We monitored cytoplasmic gene silencing using a 5′-end-capped, 3′-polyadenylated EGFP mRNA (EGFP mRNA) (5). The transfected mRNA is rapidly bound by the ribosome and remains localized in the cytoplasm, where it is transcribed to rapidly generate EGFP (5). We delivered low concentrations (10 nM) of an anti-EGFP siRNA (siRNA-GFP) or a nontargeting control (siRNA-Cntr) to HEK293-T or HT1080 cells. The next day, cells were replated and As III was added to half of the samples. The EGFP mRNA was then delivered to the cells, and fluorescence images were acquired shortly thereafter (Fig. 3 *F* and *G*). Increased siRNA nuclear function (Fig. 3 *D* and *E*) was accompanied by decreased cytoplasmic function [Fig. 3 *F* and *G*, compare EGFP silencing in As III-untreated cells (EGFP-mRNA, siRNA-Cntr vs. siRNA-GFP; first column) with As III-treated cells (second column)]. The same phenomenon could be reproduced when delivering an EGFP-targeted ON (ON-EGFP) before the EGFP mRNA in HeLa cells (Fig. 3*C*, *Top*, compare +ON-EGFP with +ON-EGFP +As III) and HEK293-T (Fig. 3*C*, *Bottom*) cells.

Finally, to confirm that the increased nuclear function extended to endogenous miRNAs, we selected two separate systems that rely on miRNA-guided target suppression in the nucleus of the CDR-1-AS and the noncoding Malat-1 RNAs. CDR-1-AS (or ciRS-7) is the circular, naturally occurring antisense RNA product of the CDR-1 gene and acts as a sponge of cellular miR-7. This leads to increased expression of the miR-7–targeted transcripts (37–39). CDR-1-AS is, in turn, targeted in the nucleus by miR-671, whose binding supports Ago-2 cleavage and the subsequent destruction of the sponge (37). Reduction of CDR-1-AS results in destabilization of the CDR-1 sense strand, an mRNA localized to the cytoplasm (37). We predicted that treating cells with As III would result in increased migration of miR-671 to the nucleus, followed by the targeting of CDR-1-AS and the subsequent reduction of the CDR-1 mRNA. The second system we investigated is based on miR-9 regulation of Malat-1 gene expression, which has been shown to also occur in the nucleus (40). Similar to the CDR-1 mRNA, the Malat-1 RNA should be suppressed by treatment of cells with As III and the resultant shuttling of miR-9 to the nucleus. As hypothesized, both CDR-1 and Malat-1 gene expression was silenced as a function of increasing As III concentrations (0.5–1.5 μM), while the expression of HDAC-2 mRNA, which is conventionally targeted by miRNAs in the cytoplasm, did not significantly change (Fig. 4*E*).

The silencing of Malat-1 and CDR-1 was reverted by transfecting the miR-9 or miR-671 antagomir, respectively, before As III treatment (Fig. 4*F*), indicating that the miR-directed target reduction is specific.

The miR-671 degradation of the CDR-1 sponge would predictably increase the available miR-7 in the cytoplasm, thus enhancing miR-7 regulation of its targets. Under our experimental conditions, decreased CDR-1 expression was consistently

mirrored by the suppression of PAX-6 and by an increase in expression of CCND1 (Fig. 4*G*), both of which are miR7 targets (41, 42). CCND1 expression has been shown to be activated by miR7 via suppression of KLF4, a negative regulator of CCND1 expression (42, 43).

ONs and Ago-2 Colocalize in SGs and in the Nucleus. Our data support the occurrence of a YB1/Ago-2 interaction that shuttles siRNAs and miRNAs into the nucleus, likely as a mechanism of gene regulation in response to cellular stress. ONs delivered by gymnosis hijack this pathway to reach the nucleus. To examine where within the cell the interaction between ONs and this endogenous cellular pathway occurs, we delivered 5′-Cy5–labeled ONs to cells with and without As III treatment and performed an immunofluorescence assay using anti–Ago-2–specific antibodies (Fig. 5*A*).

The Cy5-ONs and Ago-2 colocalized to the perinuclear region and the nucleus, where nuclear speckles can be seen (Fig. 5*A*, *Middle*, white arrows). However, the nuclear colocalization of Ago-2 with the ONs significantly increased after As III treatment (Fig. 5*A*, *Bottom*, white arrows). Since this complex responded to cellular stress, we speculated that the structures observed in the perinuclear region of the cells largely represented SGs. YB1 and Ago-2 are known to localize with both p-bodies and SGs (27, 44), and these compartments seem to physically interact and share their contents (44, 45). Of note, we previously demonstrated substantial localization of ONs in p-bodies and in nonidentified cytoplasmic structures (5).

We visualized the SGs in HT1080 cells using an SG marker, fluorescent G3BP protein, and delivered the 5′-Cy5–labeled ONs via gymnosis. The colocalization of the 5′-Cy5–labeled ONs to the SGs, as well as their shuttling to the nucleus, was enhanced by doubling the ON concentration (from 1 to 2 μM; Fig. 5*B*, compare second and third rows) and by As III treatment (Fig. 5*B*, compare second and fourth rows).

Additional Proteins Bind to YB1/Ago-2/miRNAs to Generate a Shuttling Stress-Induced Response Complex. The YB1/Ago-2 complex, in addition to nucleolin and Ago-1 (shown in this work), would be expected to include other proteins, some of which would likely be involved in gene regulation as a response to cellular stress. These proteins would likely not have been identified in the original mass spectrometry analysis, which was not performed under stress conditions. Based on the known interactions of proteins with ONs and/or YB1 and Ago-2, we analyzed Ago-1 and Ago-2 IPs from the lysates of untreated or ON- and As III-treated cells for the presence of additional proteins present in the stress-induced response complex (SIRC) (Fig. 6 *A* and *B*).

We confirmed the interaction of Ago-2 with the Smad complex by immunoblotting the IPs with antibodies specific for Smad-1, Smad-3, and Smad-4. The binding of Smad-1 and Smad-4 to Ago-2 significantly increased upon stress [compare Fig. 6 *A* with *B*, SIRC]. The nuclear protein FUS quickly associates with cytoplasmic SG during cellular stress (46) and affects miRNA biogenesis (47). Furthermore, FUS binds to RNA and single- and double-stranded DNA.

Under normal growth conditions, there is only a minimal association of FUS with the Argonaute complex (Fig. 6*A*). Its association with Ago-2 increases upon the induction of stress (compare Fig. 6 *A*, FUS, Ago-2 IP with *B*, FUS, Ago-2 IP). This same shift in Ago-2 association could also be seen for (*i*) CTCF, a master regulator of transcription that has been shown to interact with YB1 (48) and the Smad proteins (49); (*ii*) Ago-1; and (*iii*) TNRC6A, a GW182 protein that localizes to p-bodies and is capable of shuttling active RNAi factors and miRNAs into the nucleus (2, 50). The association of Ago-2 with Smad-3 and nucleolin was not affected by stress (Fig. 6 *A* and *B*). The input controls for these experiments are shown in *SI Appendix*, Fig. S11.

Discussion

It is well established that ONs are highly potent in the cell nucleus. However, it is unclear why and how they translocate to that cellular compartment since they can effectively function in the cytoplasm (5). Because of their charge and their ensuing ability to bind heparin-binding cellular proteins, PS ONs (e.g., PS-LNA-ONs) can enter cells and hijack endogenous miRNA pathways

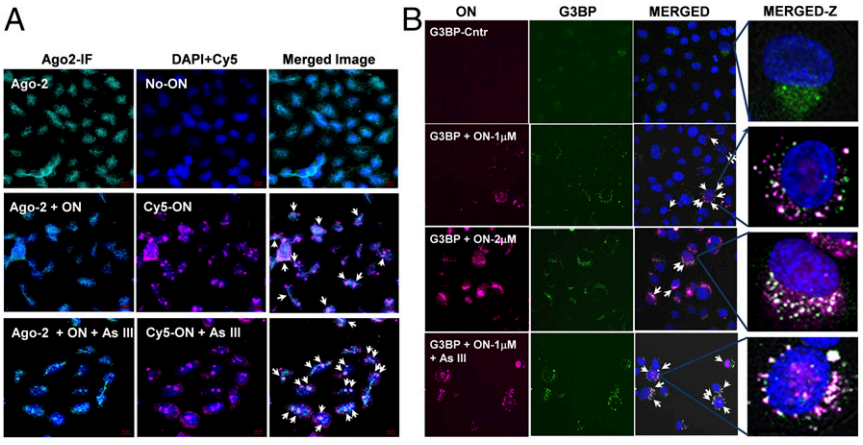

Fig. 5. ONs colocalize with Ago-2 in perinuclear SGs and in the nucleus, where they translocate as a result of As III treatment. (*A*) Immunofluorescence (IF) assay of HeLa-EGFP-654 cells treated with 1 μM SSO-654 spiked with 50 nM Cy5-labeled ON, with or without 1 μM As III treatment. Cells were fixed before Ago-2 antibody staining and confocal Z-section imaging. (*Left* and *Center*) Treatments are indicated. (*Right*) Merged images are shown. (*Top*) Ago-2 (green) cellular distribution in the absence of ON. (*Middle*) Ago-2 (green) and ON (magenta) with mostly perinuclear colocalization. This appears as a pink/white color in the merged image. (*Bottom*) Strong nuclear colocalization in cells in which the ON delivered by gymnosis was combined with As III treatment. Cell nuclei were stained by DAPI. The images were taken 24 h after ON delivery. (*B*) Perinuclear localization of the ON overlaps with G3BP, an SG marker. The first row shows a few SGs (green) in untreated HT1080 cells (G3BP-Cntr). The second row shows mostly perinuclear colocalization of 1 μM ON (magenta) with G3BP (green). The third row shows increased colocalization and when 2 μM ON was delivered to the cells. The fourth row shows the greatest ON-G3BP perinuclear and nuclear colocalization (pink/white) following As III treatment. The last column (merged-Z) for all rows shows a zoomed section (magnification: 630×) of the merged images. All micrographs are confocal Z-section images. White arrows highlight colocalization. (Magnification: 400×.)

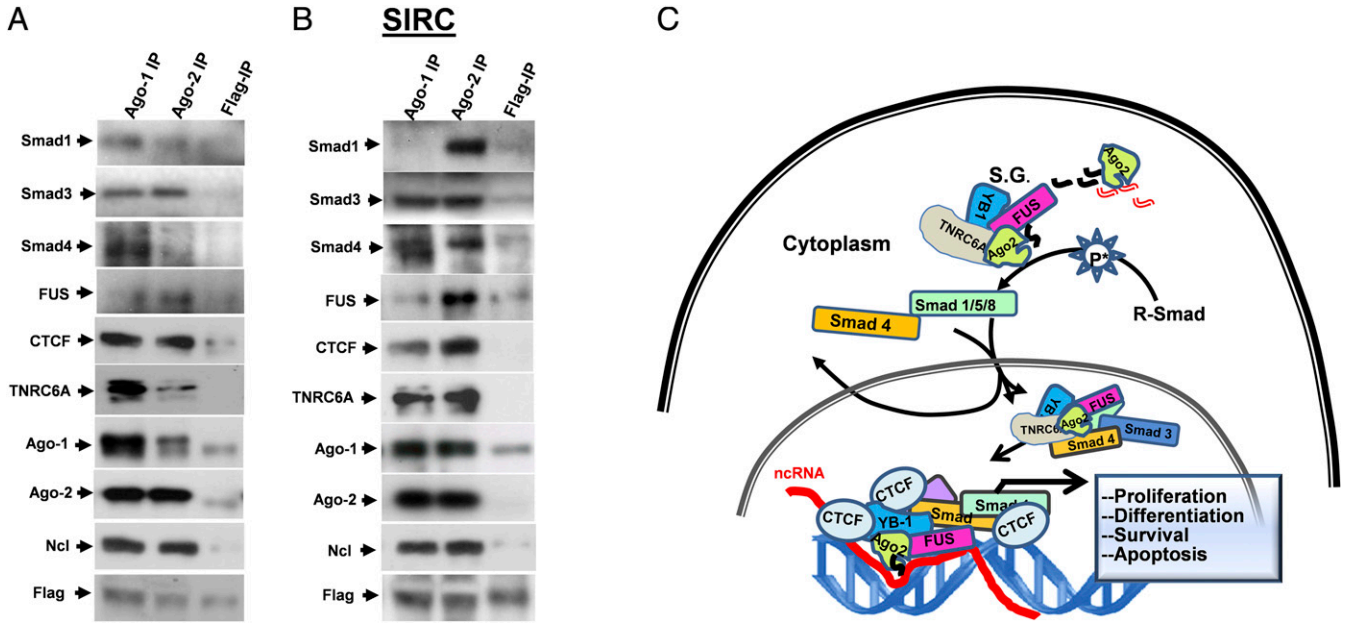

Fig. 6. SIRC includes Argonautes, transcription factors, and splicing regulators. (*A*) Anti-Flag antibodies were used to immunoprecipitate Ago-1, Ago-2, and the Flag-control from lysates of cells maintained under normal growth conditions. Specific antibodies were used to detect the presence of additional proteins, as indicated. (*B*) Experiment shown in *A* was performed in parallel using lysates of cells grown under stress conditions. (*C*) Model of SIRC assembly in which cellular stress (also caused by delivery of ONs and siRNAs) leads to localization of ON, siRNAs, and miRNAs first to SGs and then to cell nuclei.

(5). The miRNAs also shuttle to and function in the nuclear compartment (3, 51). A small miRNA subset has been proven to participate in the cellular stress response (52).

In this work, we show that the translocation of these small nucleic acids into the nucleus seems to be a general response to cell stress, which triggers formation of the SIRC. This complex contains both shuttling and gene expression modulator proteins (Fig. 6 and *SI Appendix*, Fig. S11). We also established an interaction between Ago-2 and YB1 (Fig. 1) that increases as a response to cell stress (Fig. 2) and leads to the translocation of the SIRC into the nucleus (Figs. 2, 4, and 5). The SIRC may include miRNAs and ONs (Figs. 4 and 5); a surge in nuclear shuttling corresponds to a proportional rise in the nuclear function of ONs, siRNAs, and miRNAs (Figs. 3 and 4 and *SI Appendix*, Figs. S5, S6, and S8). The cytoplasmic function of ONs and siRNAs appears to decline concomitantly (Figs. 3 and 4). The loss of cytoplasmic miRNA potency is consistent with the previously observed nuclear relocalization of Ago-2 and decreased cytoplasmic RNAi, all of which are linked to cell stress (53). Our results also support the initial formation of the SIRC, including the binding to ONs, and possibly to miRNAs, to be occurring in cytoplasmic SGs (Fig. 5*B*). The data reported in this work could help explain why the intracellular localization of ONs appears to be different based on the mode of delivery. Gymnosis (which, by itself, at lower ON concentrations and shorter treatment times is not a significant stressor) results in predominantly perinuclear localization of the ONs. This is in contrast to lipofection, which is a potent cell stressor, and directs the ONs to the nucleus (5).

We propose a model (Fig. 6*C*) in which cell stress induced by ONs and/or As III treatment leads to the formation of SGs, where the interaction between the ONs, siRNAs, or miRNAs with Ago-2, YB1, FUS, and TNRC6A first occurs. Consistent with this model is the observation that the binding of FUS and TNRC6A to Ago-2 increases upon cell stress (Fig. 6). Notably, TNRC6A has been proposed to mediate miRNA-directed nuclear silencing by transporting Ago-2 to the nucleus (50) and its return to the cytoplasm via a CRM1 (Exportin1) interaction (50). We previously reported that mature, shuttling miRNAs also return to the cytoplasm via CRM1 (51).

We suggest that cell stress leads to phosphorylation of the R-Smads (Smad-1/5/8) and their binding to Smad-4 (30) and the SIRC, followed by the nuclear relocalization of this complex (Fig. 6*C*). Smad-1 has also been shown to interact with CRM1 (54). Once in the nucleus, Smad-4 binds Smad-3, normally found predominantly in the nucleus. Subsequent to this binding, Smad-4 could be retained in this compartment (30), together with the SIRC (Fig. 6*C*).

Smad-1 and Smad-4 are important transcription regulators that can induce or repress a number of transcripts. These proteins, together with CTCF, a master regulator of transcription, would allow the cell to have a wide-ranging stress response, which we speculate may include chromatin remodeling. It is interesting to point out that the TNRC6 family contains homologies to domains of the *Schizosaccharomyces pombe* Tas3 and Chp1 proteins, which are part of the RNA-induced transcriptional silencing complex (55). Further investigation is needed, however, to confirm the existence and validity of this model as a general cell stress response mechanism.

miRNAs play crucial roles in modulating gene expression. Their deregulation has been shown to be a hallmark of cancer and other diseases. Furthermore, nuclear long ncRNAs like Malat-1 have been implicated in promoting tumor metastasis (56) and are promising therapeutic targets for the inhibition of tumor progression. We have shown that small, and thus clinically relevant, concentrations of As III can induce SIRC formation and can shuttle siRNAs, miRNAs, and ONs delivered by gymnosis to the cell nucleus. As a result, the potency of nuclear targeting is significantly increased by As III treatment. This is also an important finding with respect to ONs, whose gene silencing function relies on nuclear RNase-H activity. Improving nuclear targeting by increasing their local concentration could diminish the need for escalating ON doses, which may result in toxicity. A combinatorial strategy employing small nucleic acids and As III may have therapeutic potential, considering that As

III at low concentrations is a U.S. Food and Drug Administration-approved antileukemia drug (33, 57).

Materials and Methods

Cells, Culture Conditions, and Reagents. For most of the experiments, cells were grown in DMEM (Media Tech/Cellgro) supplemented with 10% FCS (Gemini), 1 mM L-glutamine, and 10% nonessential amino acids. The prostate cancer cell lines LNCaP were grown in RPMI 1640 (Media Tech/Cellgro) supplemented with 10% FBS and 2 mM L-glutamine. Cultures of all cell lines were maintained at 37 °C in a humidified 5% CO_2 incubator.

Cells were seeded at ∼50% confluency 24 h before treatment or seeded at 80% confluency for immediate treatment. Varying concentrations of ONs, as indicated above, were added to the culture medium for gymnotic delivery or, alternatively, for transfection as indicated below. The cells were further incubated for 48 h, after which time they were collected for analyses. The HEK293 Tet-inducible cells were seeded in six-well plates at 50% confluency in DMEM [Media Tech/Cellgro containing 10% Tet-free FBS (Clontech)]. Twenty-four hours after seeding, cells were treated with doxycycline (5 μg/mL) for an additional 48 h. The medium was then replaced, and 1 μM ON (ON-1) was added. Six hours later, the doxycycline was reintroduced, and cells were collected and fractionated after an additional 48-h incubation. The experiment was confirmed with a different ON (ON-2) nontargeting sequence. All ONs were PS-LNA–modified. The 2′O-methyl modifications were incorporated into the last two nucleotides (overhangs) of the siRNAs and into every nucleotide of the antagomirs to improve target binding and/or the stability of the RNA duplex. The sequences of the miRNA probes are fully complementary to the antisense (active) miRNA strand. All other ON sequences used in this work are listed in *SI Appendix*, Table S1.

AS III (As_2O_3) was purchased from Sigma–Aldrich and dissolved in a minimal volume of 1 M sodium hydroxide (NaOH). The arsenite solution (referred to as As III) was then diluted with PBS to a 10 mM concentration and used as a stock solution.

GFP (sc-9996), FUS/TLS (sc-373888), and SMAD4 (sc-7967) antibodies were purchased from Santa Cruz Biotechnology; anti–α-tubulin antibody was purchased from Sigma–Aldrich; and c-myc antibody was purchased from Thermo Fisher (MA1-980). The nucleolin (ab22758), TCP1 (ab92746), CTCF (ab70303), YB1 (ab76149), SMAD3 (ab40854), Ago-2 (ab57113), SMAD1 (ab126761), CBX1/HP1 beta (ab10478), and KU-70 (ab108604) antibodies were purchased from Abcam; the Ago 1 (04-083 6d8.2) antibody was purchased from EMD Millipore; the FLAG (8146S) antibody was purchased from Cell Signaling; and the TNRC6A antibody was purchased from Bethyl Laboratories. The PLA antibodies were anti-YB1 (ab12148; Abcam) and anti–Ago-1 (015-22411; Wako) or anti–Ago-2 (011-22033; Wako and ab57113; Abcam). Secondary antibodies against rabbit (sc-2370) and mouse (sc-2060) primary antibodies were obtained from Santa Cruz Biotechnology.

Plasmids, siRNA, mRNA Transfections, and Gymnotic Delivery of ONs. Cell were seeded at 50% confluency in DMEM containing 10% FBS 24 h before transfection. Five micrograms of the various plasmids per six-well dish was transfected using Lipofectamine 2000 or 3000 (Life Technology) as recommended by the manufacturer. The siRNAs were delivered at a final concentration of 20–50 nM using TransIT siQUEST (Mirus Bio LLC) or Lipofectamine 3000 through a reverse-transfection procedure, as recommended by the manufacturers. For the experiment shown in Fig. 3 *F* and *G*, 40 nM anti-EGFP siRNA or a nontargeting siRNA control were reverse-transfected into HT1080 or HEK293-T cells for 5–6 h, after which the medium was removed and cells were washed two to three times with PBS. Fresh medium with or without 1.5 μM As III was then added to half of the samples for overnight treatment. Following this treatment, the As III was removed by washing the cells once with PBS and adding fresh medium. One hundred nanograms of EGFP mRNA was immediately delivered to the cells with Lipofectamine 2000 for 4 h, after which fluorescence images were acquired with an EVOS FL cell imaging microscope (Thermo Fisher). A similar protocol was used for the ONs (Fig. 3*C*). ONs were delivered via gymnosis to HeLa or HEK293-T cells at ∼50% confluency, immediately after seeding the cells, at a concentration of 1 μM. After ∼18 h, the cells were lifted and reseeded in 96-well plates. Half of the samples were treated with 1.5 μM As III and incubated overnight. The following day, cells were washed with PBS to remove the As III, incubated for ∼30 min with fresh medium, and transfected with 100 ng of EGFP mRNA (complexed with Lipofectamine 2000) for 3 h. After this time, cells were washed with PBS; fresh medium, with or without As III, was added for an additional 5-h incubation. Fluorescence images were acquired with an EVOS FL cell imaging microscope. In all other experiments where As III treatment was performed, the As III was added to the cells at the time of seeding. In our experimental systems, 1–1.5 μM concentrations of As III consistently gave the best results. However, optimal concentrations and time of treatment could vary based on the cell line used and must be determined empirically.

Cytoplasmic and Nuclear Fractionations. Cells were briefly treated with trypsin-EDTA and gently resuspended in DMEM. They were then spun down in Falcon tubes for 4 min at 225 relative centrifugal force (rcf) in a Beckman tabletop centrifuge, washed once with PBS, and spun again for 5 min at 225 rcf. After completely aspirating the PBS, 800 μL of hypotonic buffer [10 mM Hepes (pH 7.9), 1.5 mM $MgCl_2$, 10 mM KCl] was added to each sample; the pellet was then gently resuspended, transferred to a microfuge tube, and placed in ice for 2 min. During the remainder of the protocol, samples were kept in ice and spun at 4 °C. Ten percent Nonidet P-40 was added to a final concentration of 0.4%. Samples were inverted several times and spun at 900 rcf for 5 min. Of the supernatants (cytoplasmic fractions), 400 μL was collected for RNA processing and ∼300 μL was processed for protein extraction. Samples were quickly spun again (900 rcf for 10 s) to remove any leftover supernatant. Then, the pellet (nuclear fraction) was gently resuspended in 500 μL of hypotonic buffer and spun at 900 rcf for 2 min. This washing step was repeated three times. At the final wash, 250 μL of hypotonic buffer was transferred to an additional a fresh microfuge tube and mixed with 250 μL of high-salt buffer [30 mM Hepes (pH 7.9), 1.5 mM $MgCl_2$, 800 mM NaCl, 0.4 mM EDTA (pH 8.0)], 4% Nonidet P-40, and freshly added Complete Mini EDTA-Free Protease Inhibitor Mixture (Roche Diagnostics); vortexed; incubated on ice for 30 min; and quickly sonicated. Samples were spun at 23,100 rcf for 30 min, and the supernatants were collected for protein analysis. The other 250 μL of the nuclear fractions in hypotonic buffer was used to extract RNA. The samples were spun down at 900 rcf for 2 min and, after removal of the supernatant, briefly spun once again to remove any remaining buffer. To obtain cytoplasmic and nuclear RNA, the fractions were processed following the RNA STAT-60 (TEL-TEST B) protocol as recommended by the manufacturer (AMS Biotechnology).

Co-IP. Stable cell lines expressing FLAG-tagged Ago-1, Ago-2, Ago-3, or Ago-4 or a control ORF-FLAG of the same size as the Ago coding sequence (Mock) were seeded at 50% confluency in 10-cm dishes. Approximately 18 h later, 1 μM ON (final concentration) was added to the medium for gymnotic delivery or lipofected as described above, with or without As III treatment. Forty-eight hours later, the medium was removed and the cells were washed twice with 10 mL of cold PBS. One milliliter of cold low-salt lysis buffer [50 mM Tris (pH 8.0), 5 mM EDTA, 10 mM NaCl, 0.1% Nonidet P-40] with 1× protease inhibitors (cOmplete Mini; Roche Diagnostics) was added to the plates. The plates were kept in ice while cells were scraped and collected into microfuge tubes. Samples were incubated in ice for 30 min and then frozen in liquid nitrogen. The samples were subsequently thawed in cool water and drawn up and down in a narrow-gauge needle (27G1/2 309602; Becton Dickinson) five to six times to ensure complete cell lysis. Cell debris was collected by spinning samples in a microfuge tube at 4 °C at top speed for 5 min. The supernatant/lysate was then transferred to a new tube.

The lysates used for the YB1 co-IPs were obtained by adding high-salt buffer [135 mM NaCl, 1% Nonidet P-40, 20 mM HCl·Tris (pH 7.5)] and 1× protease inhibitor (5056489001; Roche Diagnostics) directly to the PBS-washed cells, which were kept on ice for ∼30 min. Lysates were assayed for protein concentration using a DC Protein Assay kit (500-0111; Bio-Rad Laboratories). A total of 0.5–2 mg of protein was transferred to microfuge tubes and rotated overnight at 4 °C. The YB1-specific antibody was added at a 1:250 dilution. IgG, a nonspecific antibody of identical isotype and species, was added to the negative control samples. The Flag-Ago proteins were coimmunoprecipitated by adding 50 μL of 50% anti-Flag M2 beads (F3165; Sigma–Aldrich) to the samples as recommended by the manufacturer. The beads were pelleted by spinning at 4 °C at 685 rcf for 1 min. The supernatants were removed, and pellets were washed three times with wash buffer [50 mM Tris (pH 8.0), 5 mM EDTA, 150 mM NaCl]. After the final wash, the immunoprecipitated complex was released from the beads by adding 25 μL of 3× Flag cleaving peptide (F4799; Sigma–Aldrich) or resuspended in loading buffer. For RNA and ON analysis, the supernatants were collected by a 2-min centrifugation at 845 rcf, fractionated in 7 M urea using 8% PAGE, and transferred onto a Hybond-N+ membrane (Amersham-Pharmacia Biotech). A ^{32}P-radiolabeled 21mer probe complementary to the endogenous miRNA guide sequences or a ^{32}P-radiolabeled 16mer probe complementary to the ONs was used for the hybridization reactions, which were performed for 16 h at 37 °C. A ^{32}P-radiolabeled 25mer probe (5′-TATGGAACGCTTCTCGAATT) complementary to a sequence present in the U6 small nuclear RNA or a 21mer (5′-GGACCCTCAGATTAAAAGTCTGATGCTC) probe complementary to a sequence present in tRNAarg was used as a control to establish the purity of the nuclear-cytoplasmic fractions.

For protein analysis, samples were resuspended in 2× SDS/PAGE sample buffer [62.5 mM Tris·HCl (pH 6.8), 2% SDS, 10% (vol/vol) glycerol, 0.002% bromophenol blue, 5% 2-mercaptoethanol], boiled for 5 min, and separated by 10% SDS/PAGE. The co-IPs were performed a minimum of two times for each experiment with an identical outcome.

Western Blot Analysis. Cells were generally harvested 48 h after treatment with trypsin digestion and washed once with PBS. Cell pellets were lysed in cold radioimmunoprecipitation assay buffer (RIPA) containing protease inhibitors, sonicated for 2 s, and placed on ice for 5 min. After removal of the cell debris by centrifugation, protein concentrations were determined using a Pierce BCA Protein Assay kit (Thermo Fisher Scientific). Aliquots of cell extracts containing 25–50 μg of protein were resolved by 10% SDS/PAGE and imaged by an ECL or Odyssey system. The dilution of the various antibodies followed the manufacturers' instructions. The monoclonal mouse anti-human α-tubulin antibody (Sigma–Aldrich) was added at a 1:4,000 dilution in TBS-Tween containing 5% fat-free dry milk. The secondary ECL anti-mouse IgG-HRP (GE Health Care) whole antibody was added at a 1:7,000 dilution. Protein signals on the blot were quantified with the ImageJ program (NIH), and protein expression was normalized to control (100%). Numbers were determined using ImageQuant software in a nonsaturation range and after subtracting the background signal.

Quantitative RT-PCR. RNA was extracted from cells using RNA-STAT 60 as recommended by the manufacturer. The RNA was treated with Turbo DNase I (Ambion) to eliminate residual DNA according to the manufacturer's instructions. First-strand cDNA was obtained by reverse-transcribing 2 μg of total RNA with iScript Reverse Transcriptase (Bio-Rad). Fifty nanograms of the resulting cDNA was analyzed via quantitative RT-PCR using SsoAdvanced SYBR Green Supermix (Bio Rad) with the corresponding specific primer sets. The PCR reactions were performed for 40 cycles at an annealing temperature of 60 °C for 30 s to 1 min, followed by a melting curve analysis. The mRNA levels were normalized to the endogenous GAPDH or HPRT mRNA, which served as an internal control. Numbers were determined from the calculated threshold cycle using iCycler iQ Real-time Detection System software. Each sample was analyzed in triplicate.

Flow Cytometry Analysis and Cell Viability. Flow cytometry data were collected by a CyAn Flow Cytometer (Beckman Coulter) and were analyzed by the FlowJo program (Tree Star, Inc.) to determine fluorescence intensity vs. cell number. For cell viability assays, harvested cells were resuspended in PBS containing 1 μg/mL DAPI (Molecular Probes). Cell growth and proliferation were assayed by staining with sulforhodamine B. Absorbance determined at 510 nm by a microplate reader.

PLA. HeLa cells were fixed in 3.7% formaldehyde for 10 min at room temperature and permeabilized by 0.3% Triton X-100 solution in PBS. After washing three times with PBS, a standard PLA procedure was performed as recommended by the manufacturer (DUO92102; Sigma–Aldrich). In brief, cells were treated with blocking solution for 1 h. One of the primary antibodies (anti-YB1, anti–Ago-1, anti–Ago-2, Smad-1, or Lamina-1) was diluted 1:200 and added to the cells for an overnight incubation at 4 °C. Diluted (1:5) PLA probes were added to the cells after two consecutive 5-min washes (wash buffer A) and incubated for 1 h at 37 °C. Following an additional 5-min wash with buffer A, diluted (1:5) ligation stock was added to the samples and the incubation was extended for an additional 30 min. Cells were washed twice for 2 min with buffer A. The amplification step was performed by applying a mix of 1:5 diluted amplification stock and 1:80 diluted polymerase to the cells and incubating for 100 min at 37 °C. Cells were washed with buffer B several times and mounted for imaging using Duolink In Situ Mounting Medium with DAPI. After ∼15 min, Z-section fluorescent images were acquired with a Zeiss LSM880 confocal microscope using a Plan-Apochromat 20×/0.8 N.A. objective.

SG Imaging and Immunofluorescence. HT1080 cells were seeded on a 96-well plate and transfected with 100 ng of the pCMV6-AC-GFP plasmid expressing G3BP1 (NM_005754; OriGene), an SG marker, using Lipofectamine 3000. One micromolar Cy5-ON was delivered by gymnosis ∼2.5 h after transfection, with or without 1 μM As III. Twenty-four hours later, cells were harvested by trypsin digestion and reseeded into 24-well glass-bottomed plates (MatTeck Corporation). The As III treatment was continued for an additional 24 h, after which the cells were stained with Hoechst 33342 (Thermo Scientific Pierce) and fixed with 4% paraformaldehyde at room temperature for 10 min. Cells were washed once and stored in PBS at 4 °C. Z-section images were acquired using a Zeiss confocal microscope.

For the immunofluorescence analysis, HeLa cells were treated with 1 μM ON and 50 nM Cy5-ON, delivered by gymnosis, with or without 1 μM As III for 24 h. Cells were fixed with 4% paraformaldehyde and permeated with 0.5% Triton X-100 before antibody staining. The Ago-2 antibody (ab57113; Abcam) was used at a dilution of 1:100, and the secondary antibody (Alexa Fluor 555 conjugate, no. 4409; Cell Signaling) was used at a 1:500 dilution.

ACKNOWLEDGMENTS. We thank Dr. W. Filipowicz for the generous gift of the Tet-inducible Ago-2 kd stable cell line, Dr. R. Kole and Dr. R. L. Juliano for providing the HeLa EGFP-564 cell line, and Dr. Lucy Brown and Shaun Hsueh for their assistance with the flow cytometry. We are particularly grateful to Dr. Roger Moore and Dr. Gabriel Gugiu for their invaluable help with the mass spectrometry analyses. The Mass Spectrometry and the Flow Cytometry Cores are supported by the National Cancer Institute of the NIH under Award P30CA033572.

1. Kole R, Krainer AR, Altman S (2012) RNA therapeutics: Beyond RNA interference and antisense oligonucleotides. *Nat Rev Drug Discov* 11:125–140.
2. Gagnon KT, Li L, Chu Y, Janowski BA, Corey DR (2014) RNAi factors are present and active in human cell nuclei. *Cell Rep* 6:211–221.
3. Catalanotto C, Cogoni C, Zardo G (2016) MicroRNA in control of gene expression: An overview of nuclear functions. *Int J Mol Sci* 17:E1712.
4. Stein CA, et al. (2010) Efficient gene silencing by delivery of locked nucleic acid antisense oligonucleotides, unassisted by transfection reagents. *Nucleic Acids Res* 38:e3.
5. Castanotto D, et al. (2015) A cytoplasmic pathway for gapmer antisense oligonucleotide-mediated gene silencing in mammalian cells. *Nucleic Acids Res* 43:9350–9361.
6. Vickers TA, et al. (2003) Efficient reduction of target RNAs by small interfering RNA and RNase H-dependent antisense agents. A comparative analysis. *J Biol Chem* 278: 7108–7118.
7. Weidner DA, Valdez BC, Henning D, Greenberg S, Busch H (1995) Phosphorothioate oligonucleotides bind in a non sequence-specific manner to the nucleolar protein C23/nucleolin. *FEBS Lett* 366:146–150.
8. Liang XH, Shen W, Sun H, Prakash TP, Crooke ST (2014) TCP1 complex proteins interact with phosphorothioate oligonucleotides and can co-localize in oligonucleotide-induced nuclear bodies in mammalian cells. *Nucleic Acids Res* 42:7819–7832.
9. Christensen NK, et al. (1998) A novel class of oligonucleotide analogues containing 2′-O,3′-C-linked [3.2.0]bicycloarabinonucleoside monomers: Synthesis, thermal affinity studies, and molecular modeling. *J Am Chem Soc* 120:5458–5463.
10. Wahlestedt C, et al. (2000) Potent and nontoxic antisense oligonucleotides containing locked nucleic acids. *Proc Natl Acad Sci USA* 97:5633–5638.
11. Gama-Carvalho M, Carmo-Fonseca M (2001) The rules and roles of nucleocytoplasmic shuttling proteins. *FEBS Lett* 498:157–163.
12. Müller-McNicoll M, et al. (2016) SR proteins are NXF1 adaptors that link alternative RNA processing to mRNA export. *Genes Dev* 30:553–566.
13. Jiang B, et al. (2010) Nucleolin/C23 mediates the antiapoptotic effect of heat shock protein 70 during oxidative stress. *FEBS J* 277:642–652.
14. Tanaka T, Ohashi S, Kobayashi S (2014) Roles of YB-1 under arsenite-induced stress: Translational activation of HSP70 mRNA and control of the number of stress granules. *Biochim Biophys Acta* 1840:985–992.
15. Sorokin AV, et al. (2005) Proteasome-mediated cleavage of the Y-box-binding protein 1 is linked to DNA-damage stress response. *EMBO J* 24:3602–3612.
16. Matsumoto K, Wolffe AP (1998) Gene regulation by Y-box proteins: Coupling control of transcription and translation. *Trends Cell Biol* 8:318–323.
17. Graumann PL, Marahiel MA (1998) A superfamily of proteins that contain the cold-shock domain. *Trends Biochem Sci* 23:286–290.
18. Buchan JR, Parker R (2009) Eukaryotic stress granules: The ins and outs of translation. *Mol Cell* 36:932–941.
19. Bartoli KM, Jakovljevic J, Woolford JL, Jr, Saunders WS (2011) Kinesin molecular motor Eg5 functions during polypeptide synthesis. *Mol Biol Cell* 22:3420–3430.
20. Sasikumar AN, Perez WB, Kinzy TG (2012) The many roles of the eukaryotic elongation factor 1 complex. *Wiley Interdiscip Rev RNA* 3:543–555.
21. Pickering BF, Yu D, Van Dyke MW (2011) Nucleolin protein interacts with microprocessor complex to affect biogenesis of microRNAs 15a and 16. *J Biol Chem* 286: 44095–44103.
22. Schmitter D, et al. (2006) Effects of Dicer and Argonaute down-regulation on mRNA levels in human HEK293 cells. *Nucleic Acids Res* 34:4801–4815.
23. Bates PJ, Kahlon JB, Thomas SD, Trent JO, Miller DM (1999) Antiproliferative activity of G-rich oligonucleotides correlates with protein binding. *J Biol Chem* 274: 26369–26377.
24. Reyes-Reyes EM, Teng Y, Bates PJ (2010) A new paradigm for aptamer therapeutic AS1411 action: Uptake by macropinocytosis and its stimulation by a nucleolin-dependent mechanism. *Cancer Res* 70:8617–8629.
25. Fredriksson S, et al. (2002) Protein detection using proximity-dependent DNA ligation assays. *Nat Biotechnol* 20:473–477.
26. Leuchowius KJ, Weibrecht I, Soderberg O (2011) In situ proximity ligation assay for microscopy and flow cytometry. *Curr Protoc Cytom* Chapter 9:Unit 9.36.
27. Eliseeva IA, Kim ER, Guryanov SG, Ovchinnikov LP, Lyabin DN (2011) Y-box-binding protein 1 (YB-1) and its functions. *Biochemistry (Mosc)* 76:1402–1433.

28. Emde A, Hornstein E (2014) miRNAs at the interface of cellular stress and disease. *EMBO J* 33:1428–1437.
29. Higashi K, et al. (2003) Interferon-gamma interferes with transforming growth factor-beta signaling through direct interaction of YB-1 with Smad3. *J Biol Chem* 278: 43470–43479.
30. Schmierer B, Hill CS (2007) TGFbeta-SMAD signal transduction: Molecular specificity and functional flexibility. *Nat Rev Mol Cell Biol* 8:970–982.
31. Sazani P, et al. (2001) Nuclear antisense effects of neutral, anionic and cationic oligonucleotide analogs. *Nucleic Acids Res* 29:3965–3974.
32. Lantz RC, Hays AM (2006) Role of oxidative stress in arsenic-induced toxicity. *Drug Metab Rev* 38:791–804.
33. Thomas X, Troncy J (2009) Arsenic: A beneficial therapeutic poison–A historical overview. *Adler Mus Bull* 35:3–13.
34. Zhang XW, et al. (2010) Arsenic trioxide controls the fate of the PML-RARalpha oncoprotein by directly binding PML. *Science* 328:240–243.
35. Zhang X, Castanotto D, Liu X, Shemi A, Stein CA (2018) Ammonium and arsenic trioxide are potent facilitators of oligonucleotide function when delivered by gymnosis. *Nucleic Acids Res* 46:3612–3624.
36. Blenkiron C, Hurley DG, Fitzgerald S, Print CG, Lasham A (2013) Links between the oncoprotein YB-1 and small non-coding RNAs in breast cancer. *PLoS One* 8:e80171.
37. Hansen TB, et al. (2011) miRNA-dependent gene silencing involving Ago2-mediated cleavage of a circular antisense RNA. *EMBO J* 30:4414–4422.
38. Hansen TB, et al. (2013) Natural RNA circles function as efficient microRNA sponges. *Nature* 495:384–388.
39. Memczak S, et al. (2013) Circular RNAs are a large class of animal RNAs with regulatory potency. *Nature* 495:333–338.
40. Leucci E, et al. (2013) microRNA-9 targets the long non-coding RNA MALAT1 for degradation in the nucleus. *Sci Rep* 3:2535.
41. Needhamsen M, White RB, Giles KM, Dunlop SA, Thomas MG (2014) Regulation of human PAX6 expression by miR-7. *Evol Bioinform Online* 10:107–113.
42. Meza-Sosa KF, et al. (2014) MiR-7 promotes epithelial cell transformation by targeting the tumor suppressor KLF4. *PLoS One* 9:e103987.
43. Tetreault MP, Yang Y, Katz JP (2013) Krüppel-like factors in cancer. *Nat Rev Cancer* 13:701–713.
44. Kedersha N, et al. (2005) Stress granules and processing bodies are dynamically linked sites of mRNP remodeling. *J Cell Biol* 169:871–884.
45. Wilczynska A, Aigueperse C, Kress M, Dautry F, Weil D (2005) The translational regulator CPEB1 provides a link between dcp1 bodies and stress granules. *J Cell Sci* 118: 981–992.
46. Dormann D, et al. (2010) ALS-associated fused in sarcoma (FUS) mutations disrupt transportin-mediated nuclear import. *EMBO J* 29:2841–2857.
47. Morlando M, et al. (2012) FUS stimulates microRNA biogenesis by facilitating co-transcriptional Drosha recruitment. *EMBO J* 31:4502–4510.
48. Chernukhin IV, et al. (2000) Physical and functional interaction between two pluripotent proteins, the Y-box DNA/RNA-binding factor, YB-1, and the multivalent zinc finger factor, CTCF. *J Biol Chem* 275:29915–29921.
49. Bergström R, et al. (2010) Transforming growth factor beta promotes complexes between Smad proteins and the CCCTC-binding factor on the H19 imprinting control region chromatin. *J Biol Chem* 285:19727–19737.
50. Nishi K, Nishi A, Nagasawa T, Ui-Tei K (2013) Human TNRC6A is an Argonaute-navigator protein for microRNA-mediated gene silencing in the nucleus. *RNA* 19: 17–35.
51. Castanotto D, Lingeman R, Riggs AD, Rossi JJ (2009) CRM1 mediates nuclear-cytoplasmic shuttling of mature microRNAs. *Proc Natl Acad Sci USA* 106:21655–21659.
52. Leung AK, Sharp PA (2010) MicroRNA functions in stress responses. *Mol Cell* 40: 205–215.
53. Detzer A, Engel C, Wünsche W, Sczakiel G (2011) Cell stress is related to re-localization of Argonaute 2 and to decreased RNA interference in human cells. *Nucleic Acids Res* 39:2727–2741.
54. Xiao Z, Watson N, Rodriguez C, Lodish HF (2001) Nucleocytoplasmic shuttling of Smad1 conferred by its nuclear localization and nuclear export signals. *J Biol Chem* 276:39404–39410.
55. Upadhyay U, et al. (2017) Ablation of RNA interference and retrotransposons accompany acquisition and evolution of transposases to heterochromatin protein CENPB. *Mol Biol Cell* 28:1132–1146.
56. Serghiou S, Kyriakopoulou A, Ioannidis JP (2016) Long noncoding RNAs as novel predictors of survival in human cancer: A systematic review and meta-analysis. *Mol Cancer* 15:50.
57. Chen SJ, et al. (2011) From an old remedy to a magic bullet: Molecular mechanisms underlying the therapeutic effects of arsenic in fighting leukemia. *Blood* 117: 6425–6437.